Research in Astronomy and Astrophysics, 25:085005 (10pp), 2025 August

https://doi.org/10.1088/1674-4527/addeb3
CSTR: 32081.14.RAA.addeb3

Research on Beam Calibration Technology of Phased Array Feed

Kai Wang[1,2], Liang Cao[1,2], Hao Yan[1,2,3], Xue-Feng Duan[1,2], Jun Ma[1,2], Mao-Zheng Chen[1,2], and Jia-Hui Li[1,2]
[1] Xinjiang Astronomical Observatory, Chinese Academy of Sciences, Urumqi 830011, China; wangkai@xao.ac.cn, yanhao@xao.ac.cn
[2] Xinjiang Key Laboratory of Microwave Technology, Urumqi 830011, China
[3] University of Chinese Academy of Sciences, Beijing 100049, China
Received 2025 February 27; revised 2025 April 29; accepted 2025 May 18; published 2025 June 25

Abstract

The most significant distinction between Phased Array Feed (PAF) and traditional multi-beam receivers lies in its beamforming capability, where the purpose of beam calibration is to accurately determine the weighting information for each beam within the field of view. This paper first introduces the beamforming principles and algorithm classifications of PAF. Drawing on the successfully implemented PAF beam calibration schemes of Australian Square Kilometer Array Pathfinder and Aperture Tile in Focus in radio astronomy observations, we present a detailed explanation of the principles and procedures for beam calibration based on the Maximum Signal-to-Noise Ratio (Max-SNR) and Linear Constrained Minimum Variance (LCMV) algorithm. Based on the existing 1.25 GHz microstrip antenna PAF array, we designed a calibration grid comprising seven distinct directional beams and established an experimental platform for PAF array beam calibration based on an analog beamformer with the Max-SNR algorithm. Test results demonstrated a maximum gain fluctuation of 3.2 dB among the seven beams, and we further refined the weighting coefficients for each beam by selecting an appropriate gain target value and introducing a scaling factor, thereby reducing the maximum gain fluctuation between the seven beams to 1.5 dB. Building upon the Max-SNR measurements of the central axial beam's intersection points with adjacent beam patterns and their gain differentials, we implemented a recalibration of the central beam using the LCMV algorithm. This approach enforced gain consistency across predetermined directions, with test results demonstrating a reduction in the central beam's gain fluctuation from 1.6 to 0.9 dB. This research systematically validates the array-level beamforming algorithm and beam calibration scheme, offering significant guidance for future PAF receivers in areas such as beam calibration scheme selection and performance correction. Furthermore, it establishes a solid foundation for the development of advanced digital beamforming technologies with enhanced data processing ability and weighting accuracy.

Key words: telescopes – instrumentation: detectors – techniques: radial velocities

1. Introduction

Phased Array Feed (PAF) is a new receiver technology in the field of radio astronomy. It is a signal receiving technology that places a small phased array antenna at the focal plane of a radio telescope and realizes simultaneous observation of multiple continuous beams in the far field by using the beamforming network and element multiplexing function (Cappellen & Bakker 2010). As a kind of multi-beam receiver, compared with the traditional multi-beam system composed of multiple horn feeds, PAF has the advantages that adjacent beams overlap each other, and the closely connected beams in the field of view can greatly improve the observation efficiency of the telescope. At the same time, it can also adopt different beamforming algorithms to control the telescope beam in a more flexible way to meet different scientific observation needs. As shown in Figure 1, the 19-element PAF array was developed for FAST by the 54th Research Institute of China Electronics Technology Corporation (Wu 2013).

In addition to the front-end array, the beamforming network at the back end of a PAF receiver is also an indispensable part of the whole system. It can realize the weighting of the whole array, adjust the beam direction in real time, generate multiple independent beams simultaneously, and cover a larger field of view for the telescope. By optimizing the weights, suppressing interference signals in specific directions, it can ultimately improve the observation efficiency and sensitivity, and support more complex scientific goals, such as high-resolution imaging and multi-target observation. The beamforming of a PAF receiver can be specifically defined as the process of forming the received signals from multiple elements into one or more beams pointing in a specific direction by adjusting the signal weights (amplitude and phase) of each element in the array (Wijnholds et al. 2011). Its mathematical expression is shown in Equation (1):

$$y(t) = \sum_{i=1}^{N} w_i \cdot x_i(t), \quad (1)$$

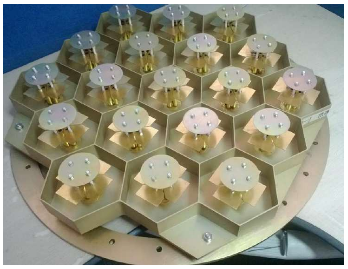

Figure 1. FAST 19-element PAF array.

where $y(t)$ is the formed beam signal, w_i is the complex weight (including amplitude and phase) of the ith element, $x_i(t)$ is the signal received by the ith element, and N is the number of elements.

The advantage of PAF lies in its ability to form multiple beams within the field of view, enabling simultaneous observation of a continuous sky area. In beamforming, multiple sets of weighting coefficients are required to generate the desired number of beams across the entire field of view. Therefore, before conducting scientific observations with a PAF receiver, it is essential to determine the weighting coefficients corresponding to each beam in the field of view. This process of solving multiple sets of weights is referred to as PAF beam calibration. Furthermore, during PAF observations, periodic calibration is necessary to correct errors, optimize performance, and improve reliability. This calibration process helps maintain the overall performance of the PAF system by addressing various factors, including gain and phase drift in each element, degradation of cross-polarization performance due to polarization leakage, field-of-view rotation during long-duration target tracking, and environmental interference (Landon et al. 2010). The Xinjiang Astronomical Observatory of the Chinese Academy of Sciences is constructing a 110 m telescope in QiTai (Wang et al. 2023), and the timely mastery of beam calibration technology is particularly critical for the successful application of the 20 cm band PAF receiver on this telescope (Wang et al. 2024a).

2. Beam Calibration Method

Since the beam calibration of PAF is the concrete realization of beamforming of the receiver system, it is necessary to understand different beamforming algorithms.

2.1. Classification of Beamforming Algorithms

Beamforming algorithms can be divided into two categories, which are data-independent and statistically optimal.

2.1.1. Data-independent Beamforming Algorithm

The data-independent beamforming algorithm is independent of array samples and solely relies on the array's steering vector. Commonly used PAF beamforming algorithms, such as the maximum directivity and conjugate field matching methods, both fall into this category. The data-independence can be understood as a fixed beamformer, which is primarily used to strictly control the beam shape without needing to adapt to environmental noise or interference, nor considering the coupling between elements. The advantages of this approach include predetermined and constant weights for the same beam, simple adjustment and independent operation of each beam. The early PHAROS2 (PHased Arrays for Reflector Observing Systems) project adopted this type of beamforming algorithm (Navarrini et al. 2019), as shown in Figure 2.

Figure 2. PHAROS2 and its beamformer.

2.1.2. Statistically Optimal Beamforming Algorithm

The statistical optimal beamforming algorithm originated from adaptive array technology (Applebaum 1976). The core principle of this algorithm is to effectively receive target signals while suppressing interference and noise, based on different optimization criteria. By utilizing the statistical characteristics of both signal and noise, the solution of the beamforming weight vector is transformed into a statistical optimization problem, thereby enabling the beam to automatically suppress interference and enhance desired signals in complex electromagnetic environments. Common optimization criteria include the Maximum Signal-to-Noise Ratio (Max-SNR), Linear Constrained Minimum Variance (LCMV), and minimum mean square error. While adaptive beamforming algorithms can enhance PAF beam performance, they require a correlator at the terminal, and the substantial amount of data acquisition increases the complexity of weight computation. Given that radio astronomy observations deal with extremely weak signals, sensitivity improvement has become the primary objective of observational equipment. Therefore, statistically optimal beamforming algorithms are particularly well-suited for radio astronomy observation requirements. The FLAG system on the Green Bank Telescope (GBT) represents an

Figure 3. FLAG assembled on GBT.

early implementation of the Max-SNR beamforming algorithm (Roshi et al. 2018), as shown in Figure 3.

2.2. Examples of Beam Calibration for PAF Receiver

Before the research on beam calibration technology of PAF, it is necessary to have a preliminary understanding of beamforming and calibration of PAF receiver which has been put into practical observation so as to carry out the next work. The related technologies of Australian SKA Pathfinder (ASKAP) and Aperture Tile in Focus (APERTIF) will be introduced respectively.

2.2.1. ASKAP

ASKAP, a Square Kilometer Array (SKA) precursor project led by the Australia Telescope National Facility (ATNF) since 2007, features a PAF array composed of patch dipole elements arranged in a 94×2 polarized rectangular configuration. Operating within the 0.7–1.8 GHz frequency range, ASKAP's digital beamforming technology enables the formation of 36 simultaneous beams, providing an instantaneous field of view of $30\,\mathrm{deg}^2$ at 1.4 GHz (Bunton et al. 2011). The PAF prototype, developed in 2015, was installed and tested on ASKAP's 12 m antenna by the end of that year, as shown in Figure 4 (Chippendale et al. 2015a and David 2017). Leveraging PAF technology, ASKAP's primary scientific objectives encompass wide-field surveys, transient source detection, and fast radio burst (FRB) localization.

For ASKAP, whose primary scientific objective is wide-field sky surveys, the corresponding PAF receiver prioritizes sensitivity in its beamforming design. Consequently, it employs the Max-SNR beamforming algorithm, optimizing the beam weight vector to maximize the ratio of signal power to noise and interference in the target direction (Chippendale et al. 2015b).

The Max-SNR algorithm, based on the fundamental definition of antenna signal-to-noise ratio (SNR), establishes the relationship between antenna SNR and beamforming factors. Through mathematical derivation, it determines the optimal SNR conditions for antenna performance, thereby calculating the corresponding beamforming weights. As an adaptive beam combining method, this approach is particularly significant for radio astronomy receiving systems that prioritize sensitivity characteristics. The SNR at the beamformer output is expressed in Equation (2):

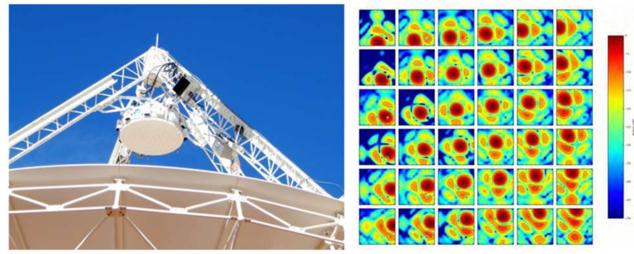

Figure 4. Mk II PAF prototype and beams test of ASKAP.

$$\mathrm{SNR} = \frac{w^H R_s w}{w^H R_n w}. \tag{2}$$

The eigenvector of the Max-SNR is obtained through the generalized eigenequation, and the beamforming weight of the Max-SNR is obtained as shown in Equation (3):

$$W_{\mathrm{msnr}} = R_n^{-1} V_s, \tag{3}$$

where R_n is the background noise correlation matrix and V_s is the signal voltage vector.

During beam calibration, based on the 36 independent beams generated by ASKAP, first, a point source with known flow density is selected as the calibration source. By rotating the radio telescope, the calibration source is located in the designed positions of the 36 beam directions, and sufficient integration time is left at each point, so as to obtain the array signal output vector $v[n]$ after the signal is superimposed with noise, as shown in Equation (4):

$$\boldsymbol{v}[n] = d[n]s + v_n[n], \tag{4}$$

where s is the signal strength of the calibration source, $v_n[n]$ is the response vector of the array to the background noise, and vector $d[n]$ is the normalized vector response of the array corresponding to the calibration source in a certain far-field direction, which is called steering vector.

In the calibration process, the telescope (array) is first pointed to the blank sky area, and the integration time is enough to obtain the response vector $v_n[n]$ to noise. At this time, the signal output vector $v[n] = v_n[n]$ of the array when observing the blank area. The selected blank region should be in close proximity to the calibration source to ensure similar noise statistics. For radio telescopes equipped with PAF systems, considering the variation in system noise temperature, the noise correlation structure depends on the elevation angle. Therefore, it is optimal to select a blank region at the same elevation but with a lateral deviation from the calibration

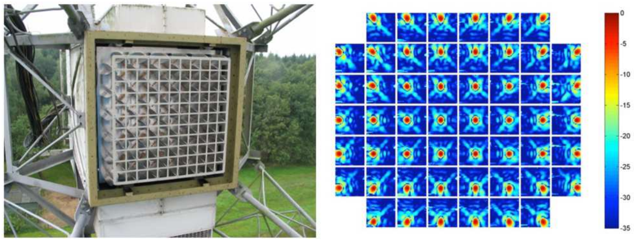

Figure 5. PAF prototype and beams test of APERTIF.

source position. The noise covariance matrix is then estimated through averaging multiple observations, as expressed in Equation (5):

$$\hat{\boldsymbol{R}}_n \approx \frac{1}{M}\sum_{n=1}^{M} \boldsymbol{v}[n]\boldsymbol{v}[n]^H \tag{5}$$

where M is the number of samples collected in the integration time, which needs to have a considerable number to realize the covariance estimation of noise.

The response vectors $v[n]$ of directions are obtained by rotating antenna. The steering vector corresponding to each beam direction can also be estimated by pointing the beam at the calibration source, integrating for a period of time, and taking multiple sets of data for average, as shown in Equation (6):

$$d[n] \approx \frac{1}{M}\sum_{n=1}^{M} v[n]. \tag{6}$$

Finally, the Max-SNR weights corresponding to the beams are related to their respective steering vectors and noise correlation matrices, as shown in Equation (7):

$$W_{\mathrm{msnr}} = R^{-1}\, d[n]. \tag{7}$$

2.2.2. APERTIF

APERTIF is a PAF development initiative launched by ASTRON (Netherlands Institute for Radio Astronomy) in 2008. The project's primary objective is the implementation of PAF receivers on the Westerbork Synthesis Radio Telescope (WSRT), operating within the 1.13–1.75 GHz frequency range. The receiver comprises an 11 * 11 array of Vivaldi antenna elements with dual-polarization design. Through digital beamforming technology, APERTIF enables the formation of 40 simultaneous beams, providing WSRT with an instantaneous field of view of 10.5 deg^2 at 1.4 GHz, as shown in Figure 5 (Cappellen et al. 2022). By APERTIF technology, WSRT's scientific objectives primarily focus on neutral hydrogen surveys, FRB and pulsar searches, and transient source monitoring.

For APERTIF, where high-resolution imaging is the main scientific goal, the sensitivity of each beam in field of view should be as uniform as possible, and anti-interference should also be considered during beamforming. The traditional Max-SNR beamformer maximizes the sensitivity in the central direction of a beam, but APERTIF uses an enhanced LCMV algorithm. This advanced approach incorporates additional constraints to ensure smoother transitions between adjacent beams and maintain more uniform sensitivity distribution across the entire field of view throughout the operational bandwidth. Furthermore, the LCMV algorithm enables direct minimization of beam sensitivity in predetermined interference directions, effectively reducing their impact on observations.

The definition of LCMV beamformer is shown in Equation (8):

$$W_{\mathrm{lcmv}} = \arg\min_{W} W^H R_{\mathrm{vv}} W. \tag{8}$$

Assuming constraint condition D is an N^*M matrix composed of M steering vectors, and constraint factor g is an M^*1 sequence, their relationship with the weights of the LCMV beamformer is $D^H w = g$. At this point, the LCMV beamforming weight under closed form can be obtained, as shown in Equation (9):

$$W_{\mathrm{lcmv}} = \boldsymbol{R}_{\mathrm{vv}}^{-1}\boldsymbol{D}[\boldsymbol{D}^H\boldsymbol{R}_{\mathrm{vv}}^{-1}\boldsymbol{D}]^{-1}\boldsymbol{g} \tag{9}$$

From Equation (9), it can be seen that both D and g can control the formed beam pattern of the array in various ways. For example, g can be set to 0 in a fixed interference direction d_s, or g can be used to control the gain fluctuations of all beams within the field of view. Generally, the number of constraint conditions should be much smaller than the number of elements, and a small portion of beamforming degrees of freedom should be used to satisfy the constraints. When the expected pattern shape is complex and requires too many constraint points, feature constraint methods can usually be used to form a reduced order D to achieve appropriate approximation of the expected pattern (Elmer et al. 2014).

When there is only one constraint condition, Equation (9) can be simplified as shown in Equation (10). It can be seen that the linear constrained minimum variance beamformer at this time is the same as the Max-SNR beamformer with a single calibration source.

$$W_{\mathrm{lcmv}} = \frac{\mathrm{g}}{d^H\boldsymbol{R}_{\mathrm{vv}}\boldsymbol{d}}\boldsymbol{R}_{\mathrm{vv}}^{-1}\boldsymbol{d} = \alpha\boldsymbol{R}_{\mathrm{n}}^{-1}\boldsymbol{d}[\mathrm{n}], \tag{10}$$

where the coefficient α is used for normalization and is generally set to 1.

In addition, when performing PAF beam calibration, APERTIF can also perform fine calibration on the basis of the original number of beams. It divides the telescope field of view into 31 * 31 grid points on average, and each grid point corresponds to a beam to achieve fine calibration (Ivashina et al. 2011). This method is beneficial for achieving high-resolution imaging in complex radio environments, but the computational complexity is higher.

Figure 6. Experimental platform of beam calibration for PAF array.

3. Experiment of PAF Beam Calibration

PAF and conventional phased array exhibit both distinctions and connections in their beamforming and calibration methodologies. While phased array primarily achieves beam steering through phase adjustment of individual elements, PAF integrated with a reflector system mainly relies on amplitude weighting across different array elements for beam steering. However, both systems require ON–OFF testing of a fixed radiation source during beam calibration to acquire weighting information for each array element. The primary differences lie in the fact that phased array calibration does not need to account for the reflector, features broader beamwidths, enables larger beam scanning angles, and is predominantly governed by phase adjustment. Nevertheless, both systems share identical fundamental principles in adaptive beamforming algorithms and beam calibration techniques. Consequently, the research on beam calibration at array level of conventional phased array holds significant instructive value for future PAF application.

3.1. Experimental Platform of Beam Calibration for PAF Array

Given the absence of a reflector antenna for conducting beam calibration experiments post-PAF array assembly, we have developed a dedicated beam calibration experimental platform specifically for PAF array testing. This platform utilizes the existing 1.25 GHz microstrip antenna PAF array and leverages the experimental facilities of the Microwave Technology Laboratory at Xinjiang Astronomical Observatory (XAO; Wang et al. 2024b).

The experimental platform consists of several key components: a 16-element microstrip antenna PAF array, a signal generator, a vector network analyzer, a transmitting antenna, a one-dimensional turntable, and a power probe, as shown in Figure 6.

The platform employs microstrip antenna elements arranged in a 4 * 4 rectangular configuration with an element spacing of 0.186 m. The array utilizes the NanShan 25 m Radio Telescope (NSRT) at XAO for off-axis one beam scanning. Signal Generation: An Agilent E8257D signal generator (250 kHz–67 GHz) provides precise reference signals for pattern measurements. Network Analysis: An Agilent E8363C vector network analyzer (10 MHz–40 GHz) acquires port-to-port vector relationships during beam calibration. Reference Transmission: A Hengda Microwave dual-ridge horn antenna (0.6–6 GHz) serves as the standard gain reference transmitter. Mechanical Positioning: A one-dimensional directional turntable provides 180-degree bidirectional rotation and precise positioning capabilities for the PAF array. Signal Detection: An Agilent power probe (DC—6 GHz) collects and records post-beamforming signals.

3.2. Beam Calibration Experiment of PAF Array

3.2.1. Obtaining Calibration Weights for Different Beams

Given the array-level nature of this beamforming experiment, we initially designed the microstrip antenna PAF array to generate seven distinct beams oriented at -30°, -20°, -10°, 0°, 10°, 20°, 30°, effectively creating a seven-point calibration grid. Following the Max SNR beamforming algorithm principle, we employed vector network analysis to acquire the signal output vectors $v[n]$ from each array port when the reference antenna was positioned at these seven angular orientations. Due to the manual data recording process for each port, implementing multiple data acquisitions for averaging as described in Equation (6) was impractical. Consequently, the steering vector $d[n]$ was calculated using Equation (11):

$$d[n] = \frac{v[n]}{\|v[n]\|},\ \|\boldsymbol{v}[n]\| = \sqrt{\sum\nolimits_{k=1}^{16} |v_k[n]|^2}. \tag{11}$$

The noise related matrix R_n can be calculated using $V_n[n]$. For a single test, since R_n is a 16 * 16 matrix, in order to reduce computational complexity, it can be simplified as a diagonal matrix, as shown in Equation (12):

$$\boldsymbol{R}_n = \mathrm{diag}(|v_1[n]|^2, |v_2[n]|^2, \cdots, |v_{16}[n]|^2). \tag{12}$$

Because there are many test and calculation results corresponding to beams in seven directions, taking the case of -30° pointing as an example, the signal output vector $V[n]$ and noise output vector $V_n[n]$ tested by PAF array corresponding to 16 ports (the test process is shown in Figure 7), as well as the calculated steering vector $d[n]$ and the Max-SNR weight W_{msnr} are listed in Table 1.

By repeating the above steps, seven groups of weights corresponding to the Max-SNR beamforming algorithm under seven directions can be obtained respectively. That is to say, the beams in their respective directions correspond to a group of Max-SNR weights, which are obtained after beam

Figure 7. Signal and noise vector acquisition.

calibration and can be directly applied to the weighting of each beam in actual observation.

3.2.2. Beamforming Measurement

Using the calibrated Max-SNR weights for the seven beams, we converted these weights into corresponding amplitude and phase information for each array element. These parameters were then applied through simulated beamforming to generate weighted beam patterns, which were subsequently measured. Figure 8 illustrates the analog beamforming network and pattern measurement platform, which consists of an attenuator (for amplitude modulation), phase shifter (for phase modulation) and signal synthesizer.

The above seven groups of weights are converted into the corresponding analog beamforming network, and the finally tested seven formed beam patterns are shown in Figure 9. At the same time, the gain and beam direction information corresponding to the seven beams are summarized in Table 2.

It can be seen from the results in Table 2 that the gain of the seven beams after calibration is about 18 dBi, and the maximum gain fluctuation is 3.2 dB. The direction of each beam is slightly different from the design direction, and the maximum deviation is $2\overset{\circ}{.}7$.

4. Discussion

Although the above work has successfully demonstrated the functionality of PAF array beam calibration, the calibrated beams still exhibit gain fluctuations and pointing deviations that require appropriate correction.

The tested 3.2 dB gain fluctuation presents a significant challenge for mapping observations, as it results in a halving of signal intensity between adjacent beams. Therefore, implementing a beam gain constraint across the field of view is essential to achieve uniform gain distribution. Under this requirement, we adopt a recalibration method that incorporates combined beam gain constraints. First, a target value is selected from the gain values of each beam that have been tested after being weighted by the Max-SNR. Then, the relationship between the target value and the gain of the remaining beams is determined to obtain their respective scaling factors. These scaling factors are subsequently used to correct the previously calculated Max-SNR weights, thereby constraining the measured gain of each beam to the target gain. The relationship between the scaling factor α and the weight correction is expressed in Equation (13):

$$\alpha = \sqrt{\frac{G_0}{G_{\rm n}}}, \quad w_k^{\rm final} = \alpha_k w_k^{\rm initial}. \tag{13}$$

In this configuration, the beam at 0° serves as the central reference among the seven beams, and its measured gain of 18.3 dBi is selected as the target gain. Using Equation (13), the corresponding scaling factors and corrected weights for each beam can be calculated accordingly.

At this stage, only amplitude correction is implemented, while phase correction remains unaddressed. Theoretically, this approach results in final beam patterns that exhibit only gain variations while maintaining consistent beam directions. However, considering the previously identified pointing deviation issues, the primary challenges stem from the adjustment precision of the phase shifters in the analog beamforming network and the tightness of each Sub-Miniature A SMA joint connection. Based on preliminary estimates, the phase error for each signal remains within 5°. Consequently, to mitigate pointing deviations, we focus on minimizing the impact of these factors on phase errors during the phase matching process.

Finally, the modified weights are translated into corresponding configurations for the analog beamforming network (while preserving the original weight information and test results for the 0° and 20° beams). The resulting seven beam patterns are summarized in Figure 10, with corresponding gain values and beam patterns detailed in Table 3.

The test results presented in Table 3 demonstrate significant improvements in beam performance following correction. The maximum gain fluctuation across all beams has been reduced to 1.5 dB, representing a notable enhancement compared to

Table 1
Response Test and Calculation Results of Each Port of the Array in the Direction of −30°

	1	2	3	4	5	6	7	8
$v[n]$	3.8846 −16.527i	−21.982 +2.042i	11.97 +2.9794i	−5.9713 −6.177i	7.6725 −13.414i	−17.367 −6.258i	7.768 +10.344i	3.5372 −10.3i
$v_n[n]$	−2.9066 +7.681i	−7.8964 +8.319i	−5.9531 +6.821i	−0.781 +6.4389i	−1.7482 +7.809i	−8.8044 +3.575i	−3.8896 +1.692i	1.6984 +7.064i
$d[n]$	0.0646 −0.2747i	−0.365 +0.0339i	0.1990 +0.049i	−0.0992 −0.102i	0.1275 −0.2230i	−0.2886 −0.104i	0.129 +0.1719i	0.0588 −0.1712i
w_{msnr}	0.0096 −0.0407i	−0.027 +0.0026i	0.0243 +0.006i	−0.0236 −0.024i	0.0199 −0.0348i	−0.032 −0.0115i	0.0718 +0.095i	0.0111 −0.0324i

	9	10	11	12	13	14	15	16
$v[n]$	3.5604 −12.925i	−19.173 −4.620i	7.660 +14.623i	2.1997 −12.09i	9.6531 −16.446i	−16.514 −3.620i	7.232 +6.5738i	−0.893 −10.861i
$v_n[n]$	−2.4544 +6.012i	−7.0331 +9.728i	−8.757 +5.975i;	0.257 +9.9741i	−4.5367 +7.821i	−7.188 +3.9102i	−2.256 +2.8141i	0.783 +6.5199i
$d[n]$	0.0592 −0.2148i	−0.3186 −0.076i	0.1273 +0.243i	0.0366 −0.209i	0.1604 −0.2733i	−0.274 −0.0602i	0.1202 +0.109i	−0.014 −0.1805i
w_{msnr}	0.0140 −0.0509i	−0.022 −0.0053i	0.011 +0.0216i	0.0037 −0.0202i	0.0196 −0.0334i	−0.041 −0.009i	0.092 +0.0839i	−0.0034- 0.042i

Table 2
Measured Gain and Pointing of Seven Beams

	−30°	−20°	−10°	0°	10°	20°	30°
Gain	16.3 dBi	19.5 dBi	17.1 dBi	18.3 dBi	18.4 dBi	18.3 dBi	18.0 dBi
Direction	−32.7°	−21.8°	−11.7°	−1.2°	9.6°	19.5°	29.1°

Figure 8. Analog beamforming network and pattern measurement platform.

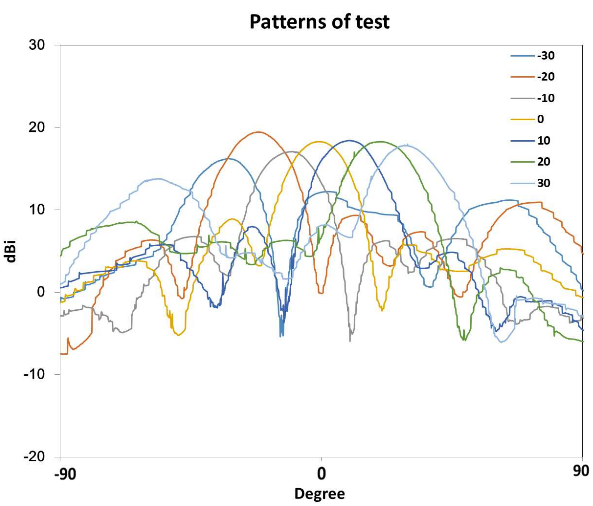

Figure 9. Test results of pattern after calibration for seven beams.

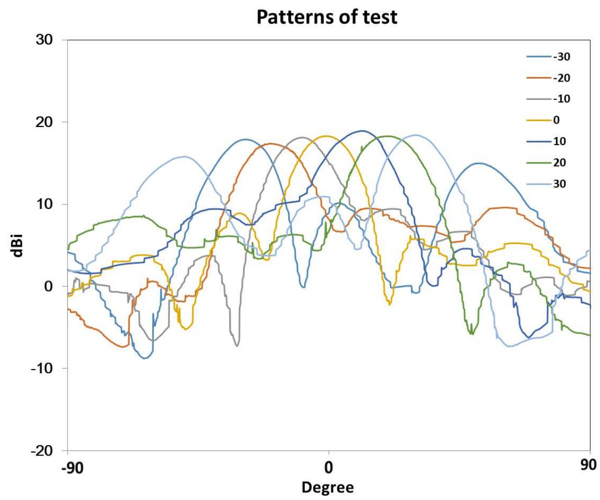

Figure 10. Test results of pattern for seven beams after gain constraint.

previous measurements. Additionally, the maximum deviation between each beam's pointing direction and its designed orientation has decreased to 1.6°. While this indicates some improvement, the hardware configuration of the analog beamforming network leads to slightly pointing correction effect and general repeatability.

Meanwhile, the LCMV algorithm was employed to calculate the weighting coefficients by incorporating the beam pattern at 0° from Figure 10. Given that this beam pattern intersects with its adjacent beams (left and right) at approximately ±7°, we designed constraints to equalize the gain of the central beam (0° beam) at three directions: −7°, 0°, 7°. The constraint factor g is expressed in Equation (14) as follows:

$$\boldsymbol{g} = [1,\ 1,\ 1]^T \tag{14}$$

In this case, the constraint matrix D is a 16×3 matrix composed of steering vectors $d(n)$ corresponding to the three specified directions (−7°, 0°, 7°), as shown in Equation (15):

$$D = [d(n_1),\ \mathrm{d}(n_2),\ \ d(n_3)]. \tag{15}$$

By separately measuring the steering vectors $d(n)$ and noise vectors $V_n[n]$ of the array at the three specified directions (−7°, 0°, 7°), and combining them with Equation (9), the weighted coefficients W_{lcmv} for the 0° beam under the LCMV algorithm can be solved.

Finally, the measured results of the 0° beam weighted by the LCMV algorithm were compared with representative cases the Max-SNR and uniformly weighted beamforming as summarized in Figure 11. Additionally, key performance metrics (gain, beam direction et al.) of the three beamforming methods are compiled in Table 4.

The test results in Table 4 demonstrate that uniform weighting achieves the highest gain (19.0 dBi), while the Max-SNR weighting provides optimal beam pointing accuracy (−0.6°). The LCMV weighting, on the other hand, achieves the lowest sidelobe level (−17.4 dB) and widest beamwidth (28.5°). Notably, although the beamwidth expansion sacrifices a small portion of

Table 3
Measured Gain and Pointing of Seven Beams After Correction

	-30°	-20°	-10°	0°	10°	20°	30°
α	1.258	0.901	1.148	1	0.988	1	1.049
Gain	17.9 dBi	17.4 dBi	18.1 dBi	18.3 dBi	18.9 dBi	18.3 dBi	19.4 dBi
Direction	$-28^\circ.4$	$-20^\circ.1$	$-9^\circ.3$	$-1^\circ.2$	$11^\circ.5$	$19^\circ.5$	$29^\circ.5$

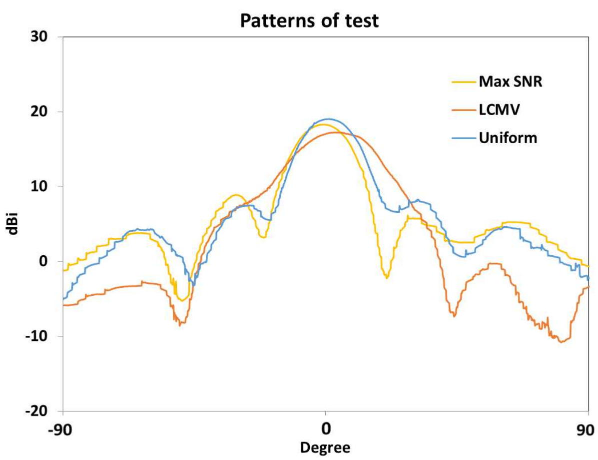

Figure 11. Measured beam patterns of the 0° beam under three beamforming algorithms.

gain, LCMV weighting effectively constrains the gain variation of the 0° beam under Max-SNR weighting at three critical directions (-7°, 0°, 7°, corresponding to the gain peak and its $\pm7^\circ$ positions) from 16.9, 18.3, 16.7 dBi to 16.3, 17.2, 16.8 dBi respectively. This reduces the gain fluctuation range from 1.6 to 0.9 dB, which will significantly benefit future PAF systems in achieving uniform sensitivity across the entire field of view.

5. Conclusion

To further investigate beam calibration methods for PAFs, analyze and correct the performance of each formed beam, this study designs a seven-beam calibration grid oriented at -30°, -20°, -10°, 0°, 10°, 20°, 30° directions. This paper is based on the 1.25 GHz microstrip antenna PAF array developed by the Microwave Technology Laboratory at Xinjiang Astronomical Observatory, Chinese Academy of Sciences. Employing the Max-SNR beam calibration scheme from the statistically optimal beamforming algorithm classification, we measured and calculated the steering vectors and weighting information for the seven beams. The beam patterns were then tested using a simulated beamforming network comprising an attenuator, phase shifter, and synthesizer, along with a pattern measurement platform. Initial test results indicated that the seven beams all achieved gains of approximately 18 dBi, with a maximum gain fluctuation of 3.2 dB and a maximum pointing deviation of $2^\circ.7$ from the designed directions. To address the requirement for beam gain uniformity in PAF field-of-view mapping observations, we proposed a beam gain constraint scheme. This approach involved selecting a target gain value and calculating corresponding gain scaling factors based on measured gain values to correct each beam's weighting coefficients, ultimately reducing the maximum gain fluctuation to 1.5 dB. While the maximum pointing deviation was also reduced to $1^\circ.6$, this pointing improvement was independent of the gain constraint scheme but highlighted the need for precise phase weighting of each signal.

Table 4
Measured Beams Performance of the 0° Beam under Three Beamforming Algorithms

	Gain/dBi	Beam Direction/$^\circ$	Beam Width/$^\circ$	Sidelobe Level/dB
Max-SNR	18.3	−0.6	19.2	−9.4
LCMV	17.2	2.7	28.5	−17.4
Uniform	19.0	1.3	19.5	−10.7

Building upon the measured Max-SNR results of the central 0° beam and its intersection points with adjacent $\pm10^\circ$ beam patterns along with their gain differences, we recalibrated the central beam using the LCMV algorithm to enforce consistent gain levels at three key directions (-7°, 0°, 7°). Test results demonstrated a reduction in the central beam's gain fluctuation from 1.6 to 0.9 dB. During this process, we conducted a comparative performance evaluation of three typical beamforming algorithms using the same PAF array. Experimental measurements revealed that: uniform weighting achieved the highest gain (19.0 dBi), Max-SNR weighting delivered optimal beam pointing accuracy ($-0^\circ.6$), while LCMV weighting attained the lowest sidelobe level (−17.4 dB) and widest beamwidth ($28^\circ.5$).

Although this research was conducted at the PAF array level, it provides significant guidance for beam calibration scheme selection and performance correction of PAF receivers at the primary focal position of radio telescopes. Future work will focus on implementing digital beamformers in conjunction with beam calibration requirements to enhance beamforming weighting accuracy and enable calibration verification for a greater number of beams.

Acknowledgments

This work was supported by the National Key R&D Program of China (2022YFC2205303), the Xinjiang Uygur Autonomous Region Tianshan Talent Training Plan (2024TSYCCX0072), the Natural Science Foundation of Xinjiang Uygur Autonomous Region (2022D01A358) and the National Natural Science Foundation of China (11973078). The work was partly supported by the Operation, Maintenance and Upgrading Fund for Astronomical Telescopes and Facility Instruments, budgeted from the Ministry of Finance of China (MOF) and administrated by Chinese Academy of Sciences.

References

Applebaum, S. P. 1976, ITAP, 24, 5

Bunton, J. D., Hampson, G., & Brown, A. 2011, in 2011 XXXth URSI General Assembly and Scientific Symp. (Piscataway, NJ: IEEE), 133

Cappellen, W. A., & Bakker, L. 2010, in 2010 IEEE Int. Symp. on Phased Array Systems and Technology, Waltham, 640

Cappellen, W. A., Oosterloo, T. A., & Verheijen, M. A. W. 2022, AJ, 62, 12

Chippendale, A. P., Brown, A. J., Beresford, R. J., et al. 2015a, in Int. Conf. on Electromagnetics in Advanced Applications (ICEAA) (Piscataway, NJ: IEEE), 541

Chippendale, A. P., Brown, A. J., Beresford, R. J., et al. 2015b, in Int. Symp. on Antennas and Propagation (ISAP) (Piscataway, NJ: IEEE), 3

David, M. 2017, in Phased Array Feed Workshop, 31

Elmer, M., Jeffs, B. D., & Warnick, K. F. 2014, ITAP, 62, 12

Ivashina, M. V., Iupikov, O., & Maaskant, R. 2011, ITAP, 59, 6

Roshi, D. A., Shillue, W., Simon, B., et al. 2018, AJ, 155, 5

Landon, J., Elmer, M., Waldron, J., et al. 2010, AJ, 139, 3

Navarrini, A., Cattani, A., & Ladu, A. 2019, in IEEE Int. Symp. on Phased Array System and Technology (PAST) (Piscataway, NJ: IEEE), 1

Wang, K., Cao, L., Ma, J., et al. 2024a, RAA, 24, 4

Wang, K., Yan, H., Ma, J., et al. 2024b, AcASn, 65, 5

Wang, N., Xu, Q., Ma, J., et al. 2023, SSPMA, 66, 8

Wijnholds, S. J., Cappellen, W. V., & Ivashina, M. V. 2011, in 30th URSI General Assembly and Scientific Symp., 1

Wu, Y. 2013, Doctoral Dissertation, Univ. Xidian